


RESEARCH ARTICLE

WILEY

Identifying individuals with Alzheimer's disease-like brains based on structural imaging in the Human Connectome Project Aging cohort

Binyin Li^{1,2,3}  | Ikbeom Jang² | Joost Riphagen^{2,4} | Randa Almkoum² | Kathryn Morrison Yochim² | Beau M. Ances⁵ | Susan Y. Bookheimer⁶ | David H. Salat^{2,3,7} | For the Alzheimer's Disease Neuroimaging Initiative

¹Department of Neurology and Institute of Neurology, Ruijin Hospital, Shanghai Jiao Tong University School of Medicine, Shanghai, China

²MGH/MIT/HMS Athinoula A. Martinos Center for Biomedical Imaging, Massachusetts General Hospital, Harvard Medical School, Charlestown, Massachusetts

³Department of Radiology, Massachusetts General Hospital, Harvard Medical School, Boston, Massachusetts

⁴Faculty of Health, Medicine and Life Sciences, School for Mental Health and Neuroscience, Alzheimer Centre Limburg, Maastricht University, Maastricht, The Netherlands

⁵Department of Psychological and Brain Sciences, Washington University in St. Louis, St. Louis, Missouri

⁶Department of Psychiatry and Biobehavioral Sciences, David Geffen School of Medicine at UCLA, University of California, Los Angeles, California

⁷Neuroimaging Research for Veterans Center, VA Boston Healthcare System, Boston, Massachusetts

Correspondence

Binyin Li, Department of Neurology and Institute of Neurology, Ruijin Hospital, Shanghai Jiao Tong University School of Medicine, Shanghai, 200025, China.
Email: libinyin@126.com

Funding information

Shanghai Rising-Star Program, Grant/Award Number: 21QA1405800; University of Minnesota Medical School; McDonnell Center for Systems Neuroscience; NIH Blueprint for Neuroscience Research, Grant/Award Numbers: U01AG052564, U01AG052564-S1; Northern California Institute for Research and Education; Foundation for the National Institutes of Health; Canadian Institutes of Health Research; Transition Therapeutics.; Takeda Pharmaceutical Company; Servier; Piramal Imaging; Pfizer Inc.; Novartis Pharmaceuticals Corporation; Neurotrack Technologies; NeuroRx Research; Meso Scale Diagnostics, LLC; Merck & Co., Inc.; Lundbeck; Lumosity; Johnson & Johnson Pharmaceutical Research & Development LLC; Janssen Alzheimer Immunotherapy Research & Development, LLC.; IXICO Ltd.; GE Healthcare; Fujirebio Europe; Genentech, Inc.; F. Hoffmann-La Roche Ltd; EuroImmun,

Abstract

Given the difficulty in factoring out typical age effects from subtle Alzheimer's disease (AD) effects on brain structure, identification of very early, as well as younger preclinical "at-risk" individuals has unique challenges. We examined whether age-correction procedures could be used to better identify individuals at very early potential risk from adults who did not have any existing cognitive diagnosis. First, we obtained cross-sectional age effects for each structural feature using data from a selected portion of the Human Connectome Project Aging (HCP-A) cohort. After age detrending, we weighted AD structural deterioration with patterns quantified from data of the Alzheimer's Disease Neuroimaging Initiative. Support vector machine was then used to classify individuals with brains that most resembled atrophy in AD across the entire HCP-A sample. Additionally, we iteratively adjusted the pipeline by removing individuals classified as AD-like from the HCP-A cohort to minimize atypical brain structural contributions to the age detrending. The classifier had a mean cross-validation accuracy of 94.0% for AD recognition. It also could identify mild cognitive impairment with more severe AD-specific biomarkers and worse cognition. In an independent HCP-A cohort, 8.8% were identified as AD-like, and they trended toward worse cognition. An "AD risk" score derived from the machine learning models also significantly correlated with cognition. This work provides a proof of

Complete listing of ADNI investigators can be found in the Data availability statement

This is an open access article under the terms of the Creative Commons Attribution-NonCommercial License, which permits use, distribution and reproduction in any medium, provided the original work is properly cited and is not used for commercial purposes.

© 2021 The Authors. *Human Brain Mapping* published by Wiley Periodicals LLC.

Lübeck, Germany; Eli Lilly and Company; Elan Pharmaceuticals, Inc.; Eisai Inc.; Cogstate; CereSpir, Inc.; Bristol-Myers Squibb; Biogen; BioClinica, Inc.; Araclon Biotech; Alzheimer's Drug Discovery Foundation; Alzheimer's Association; AbbVie; National Institute of Biomedical Imaging and Bioengineering; National Institute on Aging; Department of Defense, Grant/Award Number: W81XWH-12-2-0012; Alzheimer's Disease Neuroimaging Initiative (ADNI)

concept for the potential to use structural brain imaging to identify asymptomatic individuals at young ages who show structural brain patterns similar to AD and are potentially at risk for a future clinical disorder.

KEYWORDS

aging, Alzheimer's disease, classifier, machine learning

1 | INTRODUCTION

Alzheimer's disease (AD) pathologic and structural brain changes begin subtly, decades prior to symptom onset. β -Amyloid ($A\beta$), one of the hallmark pathologies of AD, appears 10 years or more before cognitive problems (Buchhave et al., 2012; Hanseeuw et al., 2019; Jack et al., 2019; Landau et al., 2012) and therefore could serve as an early marker of future cognitive impairment. However, currently, $A\beta$ can only be measured in the brain in vivo by positron emission tomography (PET) and it is currently clinically impractical to apply this procedure before the symptomatic stage. As an alternative, MRI is less invasive, less costly, and more available in clinical settings. Recent advances in structural brain imaging provide powerful tools for changes in the brain linked to neurodegeneration that can be used for the early identification of individuals at risk for future dementia. The combination of different structures lends itself to machine learning and multivariate data methods for AD recognition or mild cognitive impairment (MCI) prediction (Duraismy, Shanmugam, & Annamalai, 2019; Li et al., 2020; Spasov et al., 2019; Ten Kate et al., 2018; Wachinger et al., 2016). Although structural change is subtle in preclinical AD, these measures have significant relationships with local tauopathy (LaPoint et al., 2017), hypometabolism, and amyloid pathology (Benvenuto et al., 2018; Landau et al., 2012; Voevodskaya et al., 2018). These biomarkers are interactive and indicative of cognitive decline (Pettigrew et al., 2017; Wirth et al., 2013). Thus, it is possible that structural brain imaging can be used to identify individuals with slight cognitive problems, as well as individuals with specific biomarkers in the AD continuum. To date, however, structural imaging classification has primarily been applied in older samples (>55–60 years) in the age-range that is high risk for symptom expression (Belathur Suresh et al., 2018; Qiu et al., 2020; Yuan et al., 2019). The identification of “at risk” individuals who have no previous clinical diagnosis, as well as younger individuals with structural abnormalities, is more challenging as changes related to later-life disease are extremely subtle at young ages and will be difficult to distinguish from typical age-related structural change.

Recent work has demonstrated that deviation in brain structure from healthy aging is related to cognitive status (Gaser et al., 2013; Liem et al., 2017), as well as AD in the context of some genotypes (Jónsson et al., 2019; Kaufmann et al., 2019). As aging and AD have overlapping patterns of brain atrophy (Bakkour, Morris, Wolk, &

Dickerson, 2013), studies have developed robust age correction procedures for AD recognition (Dukart et al., 2011; Falahati et al., 2016; Li et al., 2020). However, to the best of our knowledge, no prior work has specifically removed age trends using an adult age-span sample and weighted AD trends to identify very early AD-like atrophy patterns in non-diagnosed and younger, asymptomatic non-clinical adults.

In this study, we examined the utility of a novel classification procedure that minimizes age effects through modeling from a large adult sample. Weighting patterns of atrophy due to AD could correctly identify individuals with subtle cognitive changes at relatively young ages using an adult cohort from the Human Connectome Project Aging (HCP-A) study (Bookheimer et al., 2019; Harms et al., 2018). The HCP-A enrolled a sample of generally healthy adults ranging from 36 to >90 years of age. A range of cognitive variation exists in the sample allowing for potential discrimination of high- and low-risk individuals from structural imaging measures spanning the wide range of the adult lifespan.

2 | MATERIALS AND METHODS

2.1 | Participants

2.1.1 | Data one (D1) for age correction

A total of 272 typically healthy adults from the HCP-A cohort were included in the study. Of these, 50% participants (136 participants, age range: 36 to >90, Table 1) were selected as D1 to model age trends in brain structure. To make full use of the wide age range of HCP-A for further age modeling and correction, we selected every other individual for D1 from the whole 272 participants which had been sorted by age. Thus, D1 and the rest HCP-A participants (D3 in Table 1) had a similar age span. HCP-A exclusion criteria include any clinical diagnosis of a cognitive or neurodegenerative disorder and therefore these participants were not considered “at risk” at enrollment. Structural brain images were acquired using T1 weighted multi-echo MPRAGE with prospective navigator motion correction (TE = 1.8/3.6/5.4/7.2 ms [multi-echo], TR = 2,500 ms, field of view = $256 \times 256 \text{ mm}^2$, number of slices = 208, voxel size = $0.8 \times 0.8 \times 0.8 \text{ mm}^3$, flip angle = 8° ; Bookheimer et al., 2019; Harms et al., 2018).

TABLE 1 Demographics from the three datasets

	D1	D2	Controls	D3
	HCP-A	AD		HCP-A
Number	136	136	268	136
Sex (female/male)	68/68	57/79	148/120	78/58
Age (year)	62.6 ± 16.6	74.2 ± 8.2	72.9 ± 6.0	62.9 ± 16.9
Education (year)	14.8 ± 4.9	15.7 ± 2.5	16.6 ± 2.5	15.8 ± 4.1
MoCA	26.2 ± 2.4	17.2 ± 4.5	25.8 ± 2.4*	26.2 ± 2.7
RAVLT	58.9 ± 13.2	22.35 ± 7.6	46.1 ± 10.2*	57.7 ± 14.1
TMT-A	35.2 ± 16.9	65.8 ± 37.3	33.1 ± 10.9*	35.2 ± 17.8
TMT-B	90.2 ± 62.4	194.4 ± 85.1	81.8 ± 41.4*	89.3 ± 103.2
A β SUVR	-	1.39 ± 0.22	1.11 ± 0.18*	-
CSF p-tau	-	383.2 ± 156.7	238.3 ± 92.7*	-
FDG SUVR	-	1.06 ± 0.15	1.32 ± 0.10*	-

Abbreviations: A β , β amyloid; CSF, cerebrospinal fluid; FDG, ¹⁸F-fluorodeoxyglucose; MoCA, Montreal cognitive assessment; p-Tau, phospho-tau; RAVLT, Rey auditory verbal learning test-immediate recall; SUVR, standardized uptake value ratio; TMT, trail-making test A and B.

* $p < .01$ for comparisons between AD and ADNI controls.

2.1.2 | Data two (D2) for AD classifier

Structural data of 136 AD and 268 normal controls (CN) from ADNI were used for AD effect estimation (Table 1). Besides cross-validation in AD/CN, we also validated the estimation by classifying 180 early MCI (EMCI) and 96 late MCI (LMCI) patients from ADNI. MRI scans were acquired on 3.0 T Siemens and GE scanners according to the ADNI-2 protocols. Siemens: 3D Magnetization Prepared-Rapid Gradient Echo (MPRAGE), TR = 2,300 ms, TE = 2.98 ms, flip angle = 9°, voxel size = 1 × 1 × 1.2 mm³. Philips: 3D MPRAGE, TR = 6.8 ms, TE = 3.1 ms, flip angle = 9°, voxel size = 1 × 1 × 1.2 mm³. GE: 3D inversion-recovery spoiled gradient-recalled (IR-SPGR), TR = 2,300 ms, TE = Min Full, flip angle = 11°, voxel size = 1 × 1 × 1.2 mm³. PET scans using ¹⁸F florbetapir (AV45) tracer were performed for imaging A β . We obtained AD-specific biomarkers (A β , CSF *phospho*-tau, and brain metabolism by ¹⁸F-fluorodeoxyglucose [FDG] PET) from the ADNIMERGE dataset (<https://adni.bitbucket.io/reference/adnimerge.html>). The averaged whole-brain standardized uptake value ratios (SUVR) for A β were calculated as mean cortical values normalized by whole cerebellum, and SUVR for FDG-PET was calculated from the averaged value of angular, temporal, and posterior cingulate cortex divided by pons/vermis (Landau et al., 2011).

2.1.3 | Data three (D3) for validation in HCP-A

Another 136 adults from the HCP-A cohort (Table 1) were used to find whether the classifier from D1 and D2 could correctly identify high AD risk individuals with subtle cognitive changes. Assessments in the HCP-A cohort included Montreal cognitive assessment (MoCA), trail-making test A/B (TMT-A/B), and Rey Auditory Verbal Learning Test (RAVLT). The MRI protocols were identical to D1.

2.2 | Structural features

The preprocessing pipeline of structural images was performed using FreeSurfer version 6.0 (<https://surfer.nmr.mgh.harvard.edu/>; Dale, Fischl, & Sereno, 1999; Fischl et al., 2002; Fischl, Sereno, & Dale, 1999) as described in our prior publications (Belathur Suresh et al., 2018; Salat et al., 2009). Processing steps included spatial and intensity normalization and skull stripping. The resulting volume was segmented into gray matter, white matter, and CSF, and a deformable surface algorithm was used to identify the pial surface. Cortical thickness was determined by measuring the distance between the white matter and pial surfaces. We extracted averaged cortical thickness in 74 labels per hemisphere from the Destrieux atlas (Destrieux, Fischl, Dale, & Halgren, 2010) respectively, and thus each participant had 148 cortical thickness features from the brain surface.

The automatic subcortical segmentation of brain volume used an atlas containing probabilistic information on the location of structures as described previously (Fischl et al., 2002). Volumes of 16 regions of interest (ROI) were extracted and corrected by total intracranial volume, including cerebellum white matter, cerebellum cortex, thalamus, caudate, putamen, pallidum, hippocampus, and amygdala in each hemisphere. A total of 164 features for each participant were used for classification.

2.3 | Age detrending

We applied the natural cubic spline regression to compute the relationship between age and each raw structural feature of D1. We placed age bins at 40, 60, and 80 throughout the full range of age to increase the flexibility of regression which could be done at each age range (younger: <40, middle-age: 40–60, old: 60–80, and oldest-old: >80). The coefficient of determination regression score (R^2) was used to evaluate each feature–age relationship. Thus, we built 164 age

models from age and 164 features in D1. We put ages from D2 and D3 into age models and got their predicted features (i.e., 164 predicted features for each participant). Age detrending was defined as the subtraction of predicted features from their real features.

After detrending, each participant had a vector of 164 residuals of fit (defined as “deviation”) which represented the features removing the age effect. Thus, there was a 136×164 final deviation matrix for AD and 268×164 deviation matrix for CN in D2.

2.4 | AD effect estimation

Feature-wise comparisons were performed on deviations between the AD and CN groups by independent two-tail *t*-tests (CN – AD). The deviation in each group was evaluated before each *t*-test. If the variances were not equal in both groups, the Welch's *t*-test was used alternatively. The *p* values from *t*-tests were corrected for multiple comparisons using the Benjamini–Hochberg procedure at the level of 0.05. The nonsignificant *t* values (corrected *p* > .05) were set as zero, and then all *t* values were standardized into the range between 1 and 2. Weighted deviation (WD) was defined as the multiplication by deviation and the corresponding *t* value. In this way, deviations that were different between AD and CN were amplified by standardized *t* values. Finally, AD had a 136×164 WD matrix and CN had a 268×164 WD matrix for the next step.

2.5 | Support vector machine classifier

Support vector machine (SVM) is a commonly utilized, supervised, and multivariate classification method. In this study, we input WDs as covariates for AD and CN, and used the SVM implementation publicly available in the scikit-learn package based on python (Pedregosa et al., 2011). We exhaustively searched the kernel functions including radial basis, linear, polynomial and sigmoid function, and their parameters (e.g., regularization parameter *C*, kernel coefficient γ) for optimal accuracy by five-fold cross-validation via grid search. During each fold, the classifier was trained using data from 80% of the participants and tested using data from the remaining 20% of the participants. The grid search range for radial basis, polynomial, and sigmoid function was performed over the ranges $C = 2^{-5}, 2^{-4}, \dots, 2^{15}$, $\gamma = 2^{-15}, 2^{-14}, \dots, 2^5$. The *C* for linear function had the range: $2^{-5}, 2^{-4}, \dots, 2^{15}$.

The optimized model from AD and CN was used to classify D1 into two groups: AD-like (ADL) and non-AD-like (NADL). As an exploratory final tuning, we iteratively repeated the above steps after removing ADL participants in D1 to minimize the impact of atypical brain structure on the quantification of age trends (Figure 1), until ADL were no longer identified in D1. The pure NADL D1 and AD/CN in D2 were finally used to build the final SVM classifier.

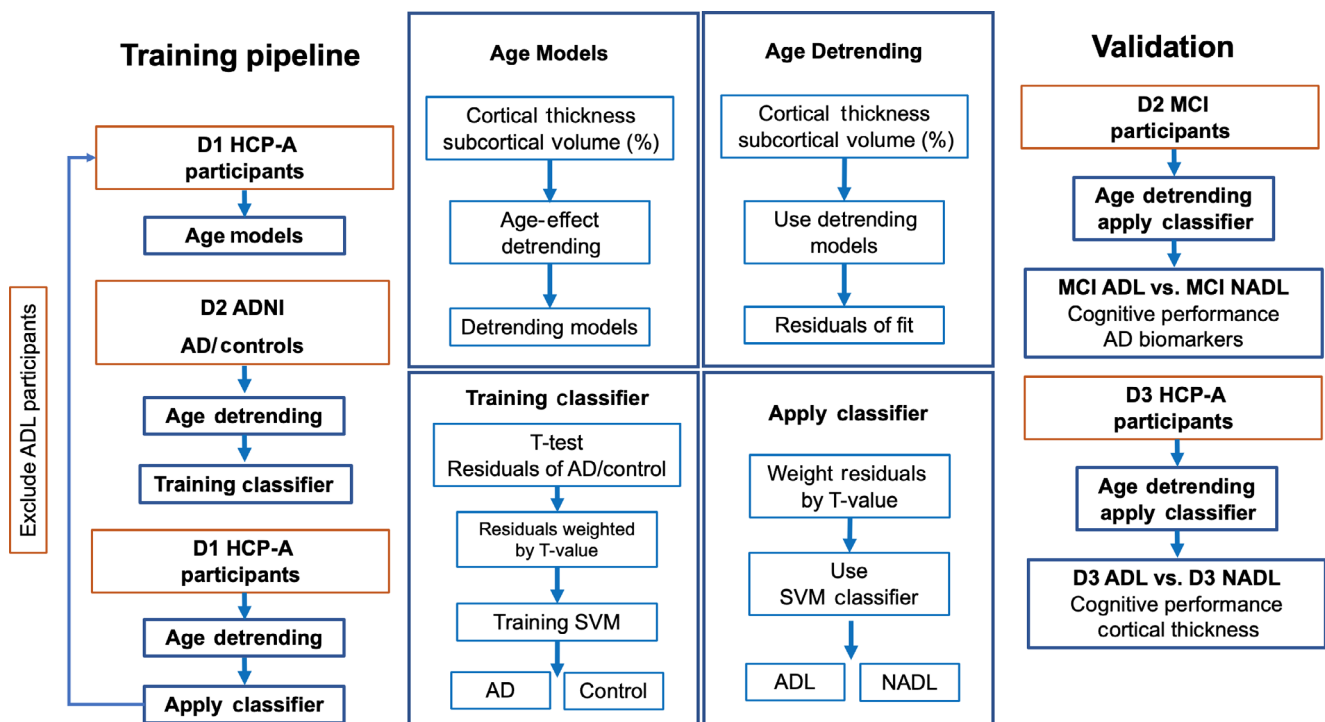


FIGURE 1 Pipeline of the study. Age models were built on HCP-A healthy participants and classifiers were trained by AD/controls. Iteration was made to exclude ADL participants from HCP-A for age detrending. AD, Alzheimer's disease; ADNI, Alzheimer's Disease Neuroimaging Initiative; HCP-A, human connectome project-aging; ADL, Alzheimer's disease-like; NADL, non-Alzheimer's disease-like

2.6 | Classifier performance

First, the classifier was applied to MCI from D2 and validated against diagnosis, biomarker, and cognitive status to demonstrate the generalizability in an earlier and more heterogeneous disease cohort. Second, the classifier was applied to D3 to determine if the classifier could identify nondiagnosed and younger at-risk individuals. In D3, ADL and NADL were compared for demographic and cognitive measures after adjusting for age effect. Finally, to validate that the results in the HCP-A sample were related to specific patterns of Alzheimer's-like atrophy as opposed to global or nonspecific atrophy, we applied a general linear model to adjust for age effect and compared vertex-wise thickness maps in the ADL to the NADL in D3.

In addition, we explored whether gender effect affected classifier performance. The subgroup of male participants ($n = 68$) in D1 was used for age modeling (Table S1). After the identical SVM training, we checked the performance of male brain-based classifier in the female participants of D2 MCI and D3 HCP-P.

To determine how age detrending and AD effect estimation improved the model, we repeated SVM and group comparisons by inputting raw features without age detrending and unweighted deviations (UD), respectively. Second, we examined whether the effects in the ADL group were specific or if individuals showing more global/nonspecific atrophy would show similar cognitive effects. In this case, the D3 participants with mean cortical thickness below the 95% confidential interval of age regression line were used as a "nonspecific global atrophy" sample to compare with the rest D3 participants. Finally, we explored the performance of other machine learning classifiers, random forest, and gradient boosting models, which were described in the Supporting Information.

3 | RESULTS

3.1 | Age detrending

In 164 natural cubic spline regressions, R^2 ranged from 0.03 to 0.54. The relationships between age and cortical thickness were more prominent ($R^2 > 0.35$) in the left superior frontal gyrus, precentral thickness, rectus gyrus, superior temporal gyrus (Figure 2), and matching patterns previously described (Salat et al., 2004). Among subcortical volumes, the cubic relationships had $R^2 > 0.35$ between age and bilateral hippocampus, amygdala, cerebellum white matter, left putamen, and pallidum.

As expected, after detrending, the deviations in CN were less correlated with age than the original features (Pearson's r : mean deviations of left hemisphere: $-.243$ vs. $-.390$; right hemisphere: $-.192$ vs. $-.335$; mean deviations of subcortical volume: $-.053$ vs. $-.458$, Figure 3). The HCP-A and CN from ADNI had generally similar deviations in the mean cortical thickness of bilateral hemispheres ($p = .043/.110$ in left/right hemisphere) and subcortical volume ($p = .666$). The deviations of cortical thickness in AD were generally more negative than those in CN (left hemisphere: $-.157$ vs. $-.029$;

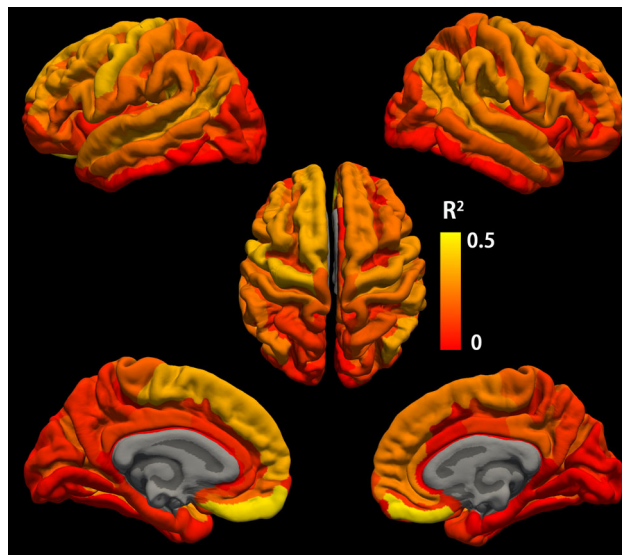


FIGURE 2 Mapping the relationships between age and cortical thickness by coefficients of determination regression score (R^2) in each parcellation from the Destrieux Atlas. The relationships were more prominent ($R^2 > 0.35$) in the left superior frontal gyrus, precentral thickness, rectus gyrus, and superior temporal gyrus

right hemisphere: $-.133$ vs. $-.021$, all $p < .001$). However, they had similar deviations in subcortical volumes ($-.004$ vs. $-.001$, $p = .123$).

3.2 | AD effect estimation

The AD and CN were similar in age, sex, and education, while AD had worse general cognition, higher A β /p-Tau and lower FDG (Table 1). As expected, after adjustment for age, AD showed regionally stereotyped cortical thinning compared to CN (Figure 4a for vertex-wise comparison) and subcortical atrophy (bilateral hippocampus, putamen, and left amygdala, ROI-wise $p < .05$ after permutation simulation correction). Several surface parcellations in AD had lower deviations than CN (Figure 4b). AD also showed greater negative deviation in the bilateral amygdala, hippocampus, pallidum, and cerebellar white matter. The extent of difference in deviation between AD and CN of each parcellation weighted the importance of deviation in AD/CN classification. In contrast to the results of deviation comparison between AD and CN listed in Section 3.1, the WDs of subcortical volumes in AD were lower than CN ($-.008$ vs. $.003$, $p = .037$).

3.3 | ADNI classification

After SVM training for the first time, we applied the classifier in D1. In 136 D1 participants, 9 (6.7%) were classified as ADL and 127 (93.3%) were classified as NADL. After excluding the nine ADLs, we repeated the SVM training in the 127 NADL. When applied to D1 again, the updated classifier recognized no more ADL participants. Thus, the final

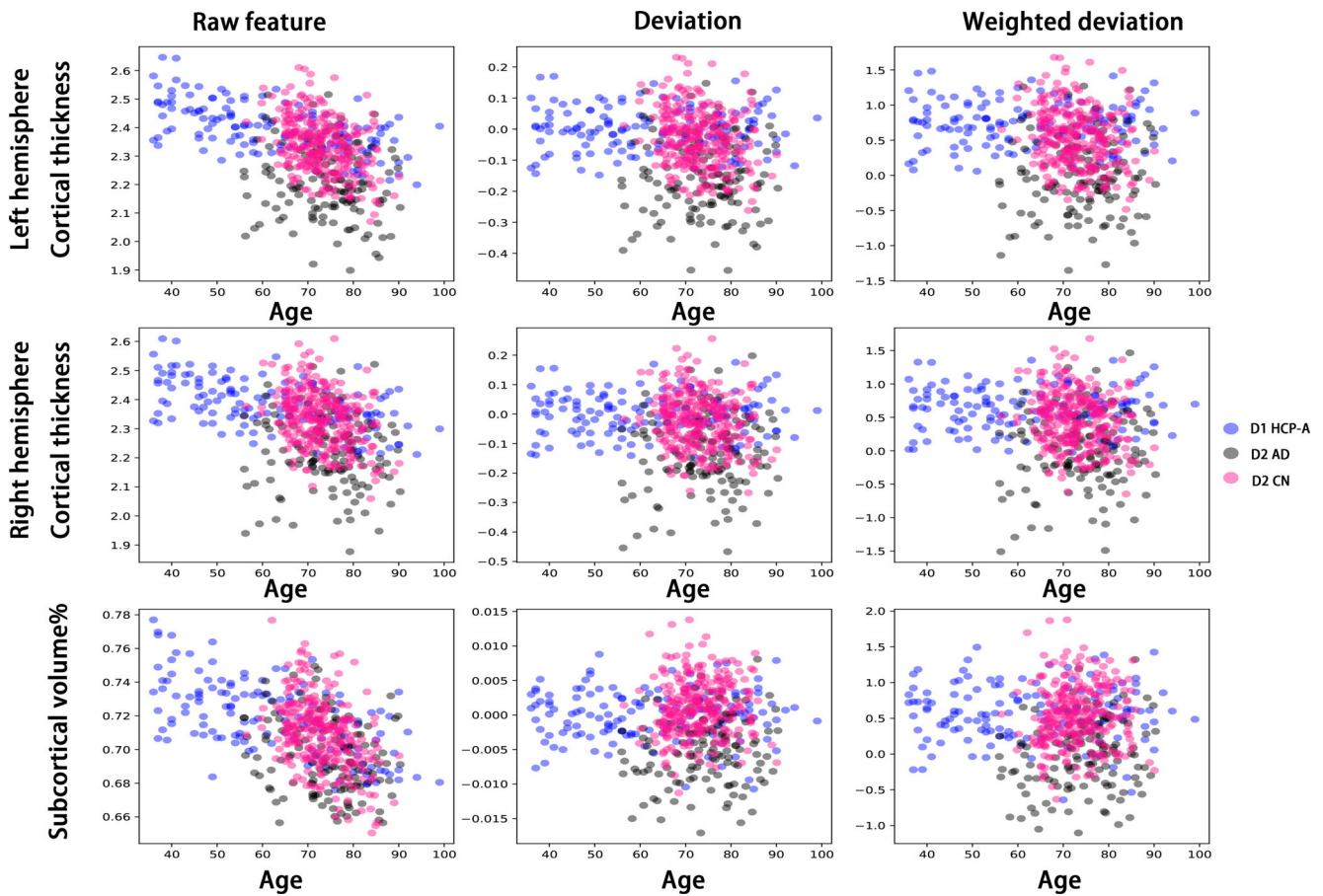


FIGURE 3 Participant-wise mean cortical thickness/subcortical volume and their deviations from age regression of AD/CN. Subcortical volumes were log-transformed and corrected by total intracranial volume. After detrending, the deviations in CN were less correlated with age than raw features. AD, Alzheimer's disease; CN, control; HCP-A, human connectome project-aging

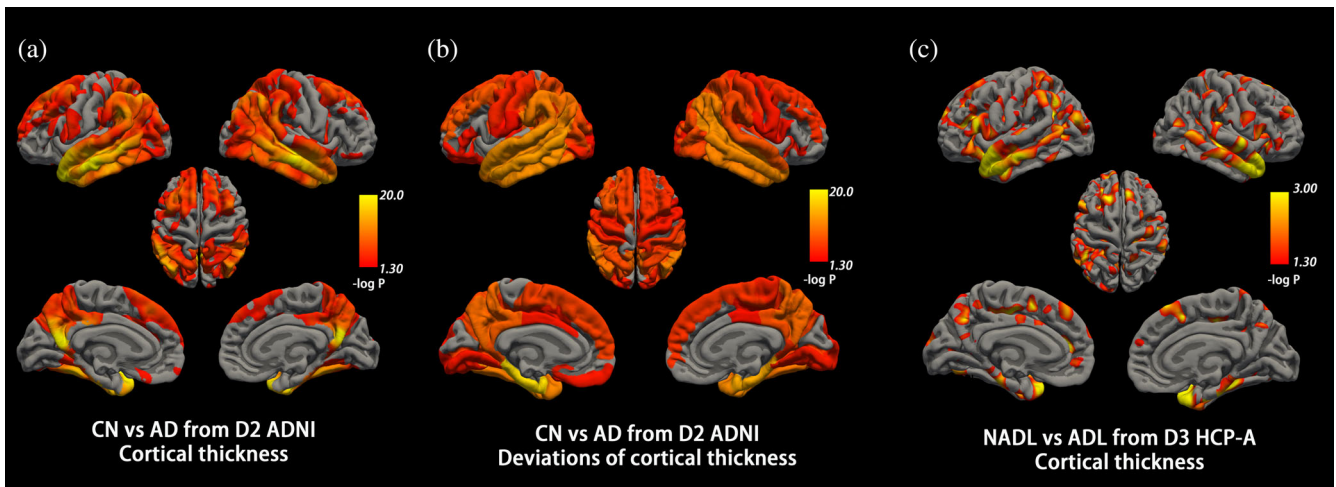


FIGURE 4 Comparison of cortical features between groups. (a) Voxel-wise comparison of cortical thickness between CN and AD, adjusting for age by the generalized linear model. (b) Parcellation-wise comparison of deviations in cortical thickness after age detrending between CN and AD. In a and b, the p values of significance were corrected by permutation simulation at level of .05. (c) Cortical thickness comparison between participants classified as ADL and NADL from HCP-A with uncorrected p values. It is important to note that this comparison includes participants across a wide adult age span (36 to >90 years), however, the group contrast shows effects similar to the cortical signature defined from older cohorts. AD, Alzheimer's disease; CN, control; HCP-A, human connectome project; ADL, Alzheimer's disease-like; NADL, non-Alzheimer's disease-like

TABLE 2 Classification results to detect AD-like individuals from ADNI MCI cohort

	EMCI		<i>p</i>	LMCI		<i>p</i>
	EMCI-ADL	EMCI-NADL		LMCI-ADL	LMCI-NADL	
Number	30	150	–	41	55	
Sex (F/M)	13/17	65/85	.840	21/20	28/27	.976
Age (year)	72.6 ± 6.0	70.2 ± 6.8	.075	72.6 ± 6.7	69.4 ± 7.3	.032
Education (year)	16.7 ± 2.6	16.1 ± 2.7	.244	16.8 ± 2.2	16.3 ± 2.5	.513
MoCA ^a	22.5 ± 2.1	24.4 ± 2.8	.001	20.8 ± 2.6	23.4 ± 3.2	<.001
RAVLT-immediate ^a	34.9 ± 5.9	39.6 ± 10.9	.026	28.5 ± 8.6	35.1 ± 10.7	.002
RAVLT-forgetting ^a	6.2 ± 2.2	3.9 ± 2.5	<.001	5.4 ± 2.1	5.2 ± 2.6	.608
TMT-A ^a	35.1 ± 13.0	36.3 ± 14.7	.829	40.8 ± 14.5	39.0 ± 14.4	.574
TMT-B ^a	103.8 ± 50.1	90.9 ± 40.8	.191	141.7 ± 85.2	96.6 ± 45.4	.005
ADAS-13 ^a	17.3 ± 5.9	11.9 ± 4.9	<.001	22.0 ± 5.8	16.7 ± 6.6	<.001

Note: Data were shown as mean ± SD. Italic values were presented for $p < .05$.

Abbreviations: ADAS, Alzheimer's disease assessment scale; ADL, Alzheimer's disease-like; EMCI, early mild cognitive impairment; LMCI, late mild cognitive impairment; MoCA, Montreal cognitive assessment; NADL, non-ADL; RAVLT, Rey auditory verbal learning test-immediate recall; TMT, trail-making test.

^aAfter adjustment for age, sex, and education.

SVM classifier was based on the 127 NADLs from D1 for age detrending and AD/CN from D2 for AD effect estimation and SVM training.

In the final SVM, the mean 10-fold cross-validation accuracy for AD/CN reached 94.0% (optimal sensitivity 95.6%, specificity 99.6%, and accuracy 98.3%) when RBF served as kernel function with $C = 2^2$ and $\gamma = 2^{-9}$. We applied the classifier in MCI of D2. In the 180 EMCI, 30 patients were classified as ADL (EMCI-ADL), and in the 96 LMCI, 41 were classified as ADL (LMCI-ADL). After adjusting for age, sex, and education, the ADL in EMCI and LMCI both had worse general cognition, memory, and trail-making speed than NADL (Table 2). For AD biomarkers, in the general linear model controlling the age and sex, the EMCI-ADL and LMCI-ADL both had significantly lower FDG SUVR (EMCI: $\beta = -.60$, $p = .002$; LMCI: $\beta = -1.10$, $p < .001$, Figure 5). Moreover, LMCI-ADL had higher β -amyloid SUVR ($\beta = .73$, $p < .001$) and CSF p-tau level ($\beta = .66$, $p = .001$). Without age detrending, the EMCI-ADL and EMCI-NADL had similar FDG SUVR ($p = .105$). The LMCI-ADL and LMCI-NADL had a smaller difference in β -amyloid SUVR ($\beta = .67$, $p = .002$) and CSF p-tau level ($\beta = .45$, $p = .042$).

3.4 | D3 HCP-A classification

We applied the final classifier in D3. Among 136 D3 participants, 12 (8.8%) were classified as D3-ADL and 124 (91.2%) were regarded as D3-NADL. The two groups were similar in age, education level, and sex (Table 3). The ADL group showed cortical thinning in bilateral middle/superior temporal gyrus, left parahippocampal gyrus, and right temporal pole, where the difference was also prominent in the AD/CN comparison here (Figure 4c) as well as described in several prior studies. Although the classifier was trained based on such patterns, these maps provide a proof of concept that individuals identified show specific

regional patterns of atrophy that are similar to the AD signature as opposed to general or global patterns of atrophy. In participants between 40–59 years of D3 ($n = 65$), five (7.7%) were classified as ADL. As expected, we observed a larger proportion of ADL participants (21.4%) in the subgroup of individuals 80+ years ($n = 28$).

After adjusting for age, D3-ADL had worse performance in trail making test-A (52.4 vs. 33.5, $p = .002$), trail making test-B (182.2 vs. 80.0, $p = .002$), and RAVLT (47.1 vs. 58.6, $p = .050$) compared to NADL by analysis of covariance (ANCOVA).

In addition, each D3 participant had a probability score of ADL and NADL derived from the SVM by scikit-learn package. We defined the ADL risk score by subtracting NADL probability score from ADL probability. AD risk was significantly correlated with MoCA ($r = -.18$, $p = .029$), TMT-A ($r = .20$, $p = .022$), and RAVLT ($r = -.30$, $p < .001$).

The classifier without age detrending showed an accuracy of 91.3% when a polynomial model served as kernel function with $C = 2^{-5}$ and $\gamma = 2^{-6}$. In D3, 26 participants (19.1%) were grouped in the AD. In contrast with the SVM model based on age detrending, the ADLs here were significantly older than NADL (74.8 ± 15.1 vs. 60.0 ± 16.1 , $p < .001$). However, after adjustment for age, we did not observe any difference in cognitive performance between ADL and NADL. Similarly, in the classifier trained from unweighted deviations, it had optimal mean accuracy of 92.1% with sigmoid kernel function of $C = 16$ and $\gamma = 2^{-6}$. The ADL from the classifier neither had a difference in cognitive performance compared to NADL (Table 3).

To test whether cortical variation among D3 affected classification, we compared the cognition between D3 participants with non-specific global atrophy to the rest of D3 sample. Six of 136 participants had mean cortical thickness below the 95% confidence interval of age regression line. The global atrophy group had lower MoCA scores (23.7 ± 3.1 vs. 26.3 ± 2.6 , $p = .026$), but the two

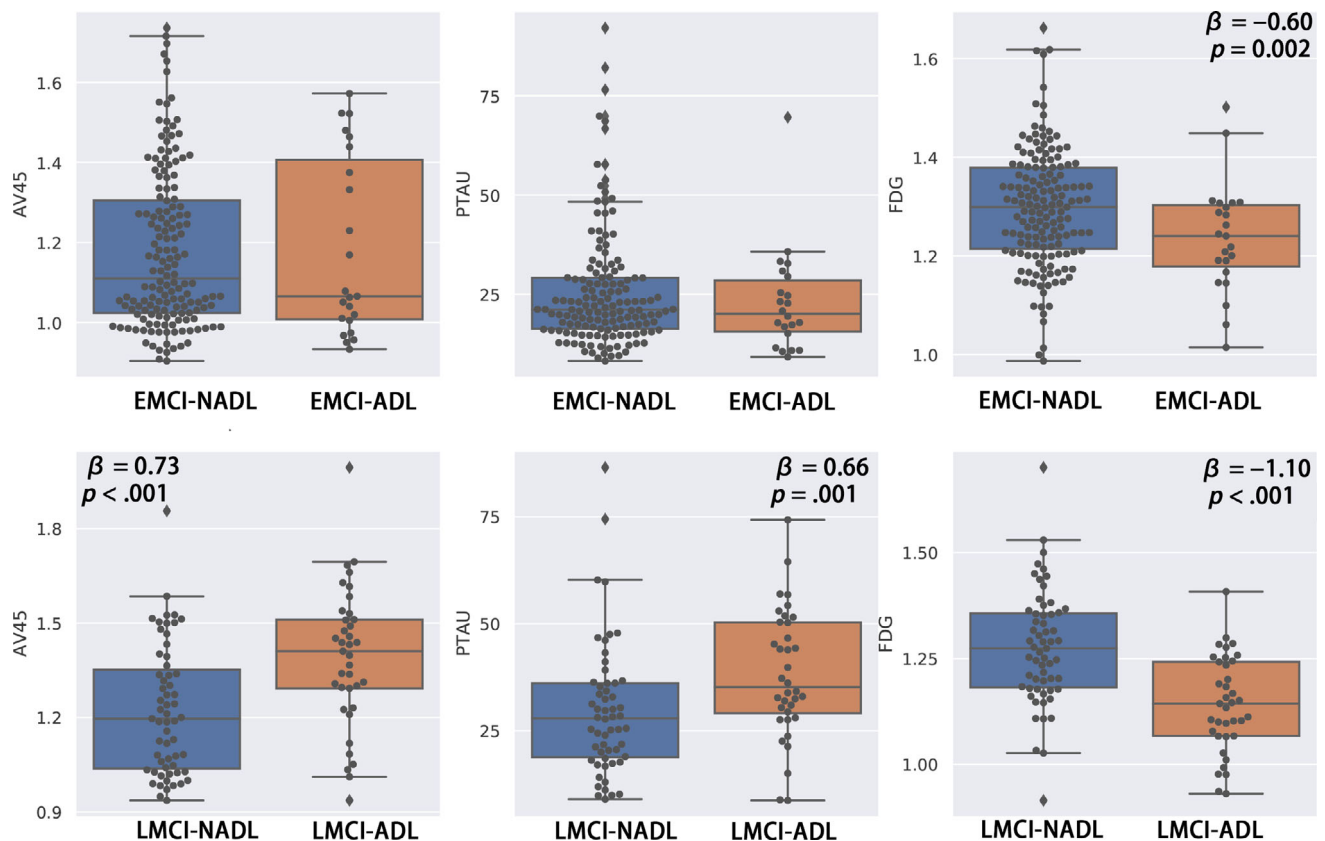


FIGURE 5 AD biomarker comparisons between MCI groups classified as ADL or NADL by the general linear model after adjusting for age, sex, and education. AV45, ^{18}F florbetapir standardized uptake value ratio for β -amyloid; PTAU, phospho-tau in cerebrospinal fluid; FDG, ^{18}F -fluorodeoxyglucose standardized uptake value ratio for glucose metabolism; EMCI, early mild cognitive impairment; LMCI, late mild cognitive impairment; ADL, Alzheimer's disease-like; NADL, non-Alzheimer's disease-like

TABLE 3 Classification results to detect AD-like individuals from D3 HCP

Feature weighting schemes	WD		UD		No detrending	
	ADL	NADL	ADL	NADL	ADL	NADL
Number	12	124	22	114	26	110
Sex (female/male)	4/8	50/74	8/14	70/44	12/14	66/44
Age (year)	70.7 \pm 22.0	62.1 \pm 16.1	68.7 \pm 16.9	61.8 \pm 16.7	74.8 \pm 15.1**	60.0 \pm 16.1
Education (year)	16.8 \pm 2.9	15.7 \pm 4.1	17.1 \pm 4.3	15.6 \pm 3.9	16.7 \pm 3.9	15.6 \pm 4.1
MoCA ^a	24.9 \pm 2.8	26.6 \pm 2.6	25.2 \pm 2.4	26.4 \pm 2.7	25.7 \pm 2.4	26.4 \pm 2.7
RAVLT ^a	47.1 \pm 9.5**	58.6 \pm 14.1	51.8 \pm 10.7	58.7 \pm 14.4	52.0 \pm 11.6	58.9 \pm 14.3
TMT-A ^a	52.4 \pm 35.9*	33.5 \pm 13.7	40.1 \pm 22.8	34.3 \pm 16.4	39.0 \pm 21.4	34.3 \pm 16.7
TMT-B ^a	182.2 \pm 296*	80.0 \pm 45.1	90.1 \pm 39.2	89.1 \pm 111.7	86.7 \pm 37.2	89.9 \pm 113.1

Note: Data were shown as mean \pm SD. * $p < .05$; ** $p < .01$ for comparisons between ADL and NADL in each model.

Abbreviations: ADL, Alzheimer's disease-like; HCP, human connectome project; MoCA, Montreal cognitive assessment; NADL, non-Alzheimer's disease-like; RAVLT, Rey auditory verbal learning test-immediate recall; TMT, trail making test; UD, unweighted deviations; WD, weighted deviations.

^aAge was adjusted in analysis of covariance.

groups were similar in RAVLT ($p = .112$), trail making test-A ($p = .326$), and trail making test-B ($p = .742$).

For the exploration of gender effect, the male brain-based SVM classifier could also identify ADL participants with lower global cognition and verbal memory, as well as higher level of AD-specific biomarkers in female MCI participants (Table S2). It could also identify

ADL in female D3 with longer trail-making time and lower MoCA (Table S3).

Gradient boosting and random forest models, in place of the SVM described, performed similarly well; identifying MCI-ADL with lower cognition as well as greater AD biomarkers (details in Tables S4 and S5). Furthermore, gradient boosting classifier found D3-ADL with

longer trail-making time and lower MoCA scores, while the random forest classifier also identified D3-ADL with differences in MoCA, TMT, and RAVLT (Table S5).

4 | DISCUSSION

We describe a proof-of-concept procedure for the classification of individuals as having AD-like brain structure that was applied in a non-clinical sample that included young and middle-aged adults. To do so, we used a large adult age-span sample to perform age correction to minimize the age effect on cortical thickness and subcortical volumes. We then weighted AD pattern of deviations after this age correction. After the first SVM classifier training, we iterated the pipeline removing any data classified as ADL to enhance the normative age estimates in NADL HCP-A participants and generated the final classifier with improved accuracy in AD/CN recognition. The procedure was validated using clinical performance as well as biomarkers in data from classically defined MCI. After this validation, we applied the classifier to an independent adult sample from the HCP-A cohort. The structurally AD-like participants from HCP-A had worse cognition, suggesting that the classifier was identifying individuals with subtle but meaningful brain changes. In contrast, when more generally selecting participants based on being below 95% age regression line (nonspecific structural abnormalities), cognitive effects were not as apparent compared to the selection of AD-specific patterns of atrophy suggesting that the effects are specific to AD atrophy patterns. These findings support the identification of individuals with ADL patterns of atrophy and subtle cognitive dysfunction in a nonclinical sample.

As age could negatively affect the performance of machine learning and multivariate models in AD recognition (Holland et al., 2012), and partially mask other disease-related factors such as ApoE genotype, global cognitive impairment, and sex (Falahati et al., 2016), we explicitly removed the age confound from the classifier based on the wide span of HCP-A age trajectory. One of the main ideas behind the detrending method was to remove age-related changes while preserving the disease-related changes for each variable separately. Gray matter volumes in most regions have linear relationship with age, and the recent study with a larger sample size also suggested that parahippocampus and temporal pole-related structural components exhibited a quadratic relationship with age (Luo et al., 2020). Compared to linear detrending (Dukart et al., 2011; Koikkalainen et al., 2012), the cubic spline regression would be more flexible than polynomial regression as it fits each age-bin with a separate model: younger (<40), middle-age (40–60), elder (60–80), and eldest elder (>80).

After age detrending, we observed that the T value weighted deviations had the strongest capability to pool individuals with worse cognition. The T values represented AD-specific features and amplified differences between AD and controls before SVM training. This approach is different from prior work which directly used SVM training for deviations without weight and had accuracy ranging from 85% to 91% (Belathur Suresh et al., 2018; Dukart et al., 2011; Li

et al., 2020), the present study introduced the AD weighting step. We compared a biomarker-based classifier using only AD positive for A β and controls negative for A β from ADNI in our previous study (Li et al., 2020). The results suggested that the clinical diagnosis from ADNI promoted more balanced sensitivity and specificity, and we also used the AD and CN group here.

However, it is important to note that there were also differences in feature selection across studies. The sensitivity and specificity were also consistent with models from the cortical thickness in AD signature regions, including hippocampus volume and global atrophy, with sensitivity from 80% to 95%, specificity from 85% to 90% (Allison et al., 2019). Importantly, the classifications found in the ADNI dataset here are likely at a ceiling performance due to potential inaccuracies in clinical labels as discussed in our prior work (Belathur Suresh et al., 2018). The multi-collinearity of age-detrended features posed arbitral variation in weight vector-based classification such as logistic regression and SVM with linear function as kernel. In our final SVM classifier, we used RBF as kernel function which is based on the distance between the data points. The input variables for model are first projected onto a higher dimensional space before they are employed in the estimation process in SVM. Multiple variables that represent the same feature of the data will be contributing more to the distance than other features, hence the model would probably be more impacted by this feature. Such SVM classification results are merely affected by collinearity (Morlini, 2006). For more reproducible results, we tried gradient boosting and random forest classifier instead of SVM and got similar classification performance.

After D3 HCP-A classification, the pattern of thickness difference between ADL and NADL D3 HCP-A groups had a similar pattern to the AD-signature cortical regions (bilateral middle/superior temporal gyrus, left parahippocampal gyrus, and right temporal pole) that were inversely correlated with the severity of clinical impairment (Dickerson et al., 2009). Moreover, the pattern was also generally in line with previous studies that found correlations between temporal/parahippocampal thinning and positive β -amyloid in MCI or healthy controls (Becker et al., 2011; Dickerson et al., 2009; Ten Kate et al., 2017).

Importantly, the structure-derived classifier provided inspection of cross-sectional AD-specific biomarkers. Reduced FDG-PET was observed in EMCI-ADL and LMCI-ADL, and the reduced general cognition and memory as well. Reduced metabolism measured by FDG and structural atrophy are both indicative of neurodegeneration in AD, and reduced FDG-PET brain metabolism predicts clinical severity and progression well (Benvenuto et al., 2018; Ewers et al., 2014). The clinical implication of detecting FDG changes was in line with the recommendation, which suggested that changes in FDG-PET track progression to clinical disease in asymptomatic biomarker-positive subjects (Dubois et al., 2016). Moreover, the A β deposition was associated with cortical thinning and lower baseline global cognition (Knopman et al., 2018), and CSF p-tau could help differentiate MCI due to Alzheimer's disease from those with stable MCI (Olsson et al., 2016). Along with these studies, our classifiers helped to find individuals with a higher level of A β and tau accumulation in MCI

population, suggesting their poor prognosis. Similarly, it also indicated faster cognitive decline in ADL from HCP-A in the longitudinal follow-up. Interestingly, FDG and structural classification were coupled in the EMCI whereas biomarkers of amyloid and tau were not coupled with these measures until LMCI. These results may suggest that structural and metabolic deficits are apparent and linked even before the accumulation of amyloid and tau pathology. Such speculation could be explored through longitudinal biomarker and cognition characterization of ADL from HCP-A, and it is being performed in ongoing work.

In addition to biomarkers, the classifier based on AD-patterns of brain structure revealed cognitive differences in MCI from ADNI, and recognized ADL in younger participants of D3 (40–59 years old). In prior studies, younger AD patients were more likely to be misclassified as controls (Dukart et al., 2011; Falahati et al., 2016). This may be due to the fact that most machine-learning/deep learning studies for AD recognition built and tested their classifiers only in participants older than 55 (Lu et al., 2018; Qiu et al., 2020). The current work demonstrates the potential to apply these procedures to detect subtle AD signals in younger nonclinical samples.

The importance of age detrending was addressed after we tested the classifier derived without age detrending. It could not differentiate FDG difference in EMCI, and its classified LMCI-ADL and LMCI-NADL had a smaller difference in AD biomarkers (lower β value in the generalized linear model) than those classified by model with age detrending. Moreover, it only identified elder ADL in D3, but with no difference in cognitive performance from NADL after adjustment for age.

We refer to this as a “proof of concept” as several limitations of the current work are being explored in ongoing research. First, HCP-A data were acquired using different imaging protocols compared to the ADNI sample, and it is possible that this could have negatively impacted performance of the classifier. As HCP-A is a community-based cohort for generally healthy participants, the HCP-A protocol did not include radioactive PET scans. Thus, we did not have AD-specific biomarkers in our validation for the final HCP-A sample. We hope to acquire and explore these markers in future studies of this cohort, especially for those who were classified as “AD-like”. However, we proved the capability of AD biomarker recognition of our classification in ADNI MCI. The classifier was built from cross-sectional data. Given differential rates of atrophy with age, it is likely that utilization of longitudinal information would improve classification performance. It is also important to note that AD is a clinically heterogeneous disease and there are atrophy subtypes (Ten Kate et al., 2018) that should be identified in future work. Finally, although cognitive effects were detected in the HCP-A sample, the 8.8% classification of ADL in HCP-A resulted in small samples of ADL within age-bins and cognitive effects were generally mild in this sample. The small sample size of HCP-A could also be impacted by other factors such as sex effects. Although the classifier was generated based on features in patients with AD biasing the identification of individuals with similar patterns, it was encouraging that the ADL participants in HCP-A showed thinning patterns similar to AD signature regions (Figure 4c) as opposed to general/global atrophy supporting the

performance of the classifier to identify this unique signature of pathology in this sample. The effects were most apparent when using the AD features and were less apparent when using a more generalized pattern of atrophy. We did not expect that cognitive differentiation would be large and these subtle effects are encouraging that the performance procedures can be successfully applied in this context. Due to practical reasons, we were not able to include the entire HCP-A sample in this study; however, we aim to further validate this approach in this larger sample in future work.

5 | CONCLUSION

We demonstrated the potential to apply machine learning a brain structural classifier to detect subtle brain and cognitive alterations in a nonclinical sample at even young ages. These results suggested that such procedures can potentially be used as a very early indicator for individuals with AD risk in relatively young community population and help screen participation in very early intervention clinical trials.

ACKNOWLEDGMENTS

We are grateful to all research participants and would like to thank our anonymous reviewers for their thoughtful comments on the manuscript. Data collection and sharing for ADNI in the study was funded by the Alzheimer's Disease Neuroimaging Initiative (ADNI) (National Institutes of Health Grant U01 AG024904) and DOD ADNI (Department of Defense award number W81XWH-12-2-0012). ADNI is funded by the National Institute on Aging, the National Institute of Biomedical Imaging and Bioengineering, and through generous contributions from the following: AbbVie, Alzheimer's Association; Alzheimer's Drug Discovery Foundation; Araclon Biotech; BioClinica, Inc.; Biogen; Bristol-Myers Squibb Company; CereSpir, Inc.; Cogstate; Eisai Inc.; Elan Pharmaceuticals, Inc.; Eli Lilly and Company; EuroImmun; F. Hoffmann-La Roche Ltd and its affiliated company Genentech, Inc.; Fujirebio; GE Healthcare; IXICO Ltd.; Janssen Alzheimer Immunotherapy Research & Development, LLC.; Johnson & Johnson Pharmaceutical Research & Development LLC; Lumosity; Lundbeck; Merck & Co., Inc.; Meso Scale Diagnostics, LLC; NeuroRx Research; Neurotrack Technologies; Novartis Pharmaceuticals Corporation; Pfizer Inc.; Piramal Imaging; Servier; Takeda Pharmaceutical Company; and Transition Therapeutics. The Canadian Institutes of Health Research is providing funds to support ADNI clinical sites in Canada. Private sector contributions are facilitated by the Foundation for the National Institutes of Health (www.fnih.org). The grantee organization is the Northern California Institute for Research and Education, and the study is coordinated by the Alzheimer's Therapeutic Research Institute at the University of Southern California. ADNI data are disseminated by the Laboratory for Neuro Imaging at the University of Southern California. The HCP-A dataset reported in this study was supported by grants U01AG052564 and U01AG052564-S1 and by the 14 NIH Institutes and Centers that support the NIH Blueprint for Neuroscience Research, by the McDonnell Center for Systems Neuroscience at

Washington University, by the Office of the Provost at Washington University, and by the University of Minnesota Medical School. This study was also supported by grants from Shanghai Rising-Star Program (21QA1405800).

CONFLICT OF INTEREST

None declared.

DATA AVAILABILITY STATEMENT

The Human Connectome Project-Aging data that support the findings of this study are available in HCP-A data at <https://www.humanconnectome.org/study/hcp-lifespan-aging> after users sign the NDA Data Use Certification (DUC) under which the data is shared. These data are released from the following resources available at: <https://www.humanconnectome.org/study/hcp-lifespan-aging/data-releases>.

ADNI Data used in preparation of this article were obtained from the Alzheimer's Disease Neuroimaging Initiative (ADNI) database (adni.loni.usc.edu). As such, the investigators within the ADNI contributed to the design and implementation of ADNI and/or provided data but did not participate in analysis or writing of this report. A complete listing of ADNI investigators can be found at: https://adni.loni.usc.edu/wp-content/uploads/how_to_apply/ADNI_Acknowledgement_List.pdf.

ORCID

Binyin Li  <https://orcid.org/0000-0003-1953-382X>

REFERENCES

- Allison, S. L., Kosciak, R. L., Cary, R. P., Jonaitis, E. M., Rowley, H. A., Chin, N. A., ... Johnson, S.C. (2019). Comparison of different MRI-based morphometric estimates for defining neurodegeneration across the Alzheimer's disease continuum. *NeuroImage*. <https://doi.org/10.1016/j.neuroimage.2019.101895>.
- Bakkour, A., Morris, J. C., Wolk, D. A., & Dickerson, B. C. (2013). The effects of aging and Alzheimer's disease on cerebral cortical anatomy: Specificity and differential relationships with cognition. *NeuroImage*, 76, 332–344.
- Becker, J. A., Hedden, T., Carmasin, J., Maye, J., Rentz, D. M., Putcha, D., ... Johnson, K. A. (2011). Amyloid-beta associated cortical thinning in clinically normal elderly. *Annals of Neurology*, 69, 1032–1042.
- Belathur Suresh, M., Fischl, B., Salat, D. H., & for the Alzheimer's Disease Neuroimaging Initiative (ADNI). (2018). Factors influencing accuracy of cortical thickness in the diagnosis of Alzheimer's disease. *Human Brain Mapping*, 39, 1500–1515.
- Benvenuto, A., Giusiano, B., Koric, L., Gueriot, C., Didic, M., Felician, O., ... Ceccaldi, M. (2018). Imaging biomarkers of neurodegeneration in Alzheimer's disease: Distinct contributions of cortical MRI atrophy and FDG-PET Hypometabolism. *Journal of Alzheimer's Disease*, 65, 1147–1157.
- Bookheimer, S. Y., Salat, D. H., Terpstra, M., Ances, B. M., Barch, D. M., Buckner, R. L., ... Yacoub, E. (2019). The lifespan human connectome project in aging: An overview. *NeuroImage*, 185, 335–348.
- Buchhave, P., Minthon, L., Zetterberg, H., Wallin, A. K., Blennow, K., & Hansson, O. (2012). Cerebrospinal fluid levels of beta-amyloid 1-42, but not of tau, are fully changed already 5 to 10 years before the onset of Alzheimer dementia. *Archives of General Psychiatry*, 69, 98–106.
- Dale, A. M., Fischl, B., & Sereno, M. I. (1999). Cortical surface-based analysis. I. Segmentation and Surface Reconstruction. *NeuroImage*, 9, 179–194.
- Destrieux, C., Fischl, B., Dale, A., & Halgren, E. (2010). Automatic parcellation of human cortical gyri and sulci using standard anatomical nomenclature. *NeuroImage*, 53, 1–15.
- Dickerson, B. C., Bakkour, A., Salat, D. H., Feczko, E., Pacheco, J., Greve, D. N., ... Buckner, R. L. (2009). The cortical signature of Alzheimer's disease: Regionally specific cortical thinning relates to symptom severity in very mild to mild AD dementia and is detectable in asymptomatic amyloid-positive individuals. *Cerebral Cortex*, 19, 497–510.
- Dubois, B., Hampel, H., Feldman, H. H., Scheltens, P., Aisen, P., Andrieu, S., ... Proceedings of the Meeting of the International Working Group (IWG) and the American Alzheimer's Association on "The Preclinical State of AD"; July 23, 2015; Washington DC, USA. (2016). Preclinical Alzheimer's disease: Definition, natural history, and diagnostic criteria. *Alzheimer's & Dementia*, 12, 292–323.
- Dukart, J., Schroeter, M. L., Mueller, K., & The Alzheimer's Disease Neuroimaging Initiative. (2011). Age correction in dementia—Matching to a healthy brain. *PLoS One*, 6, e22193.
- Duraisamy, B., Shanmugam, J. V., & Annamalai, J. (2019). Alzheimer disease detection from structural MR images using FCM based weighted probabilistic neural network. *Brain Imaging and Behavior*, 13, 87–110.
- Ewers, M., Brendel, M., Rizk-Jackson, A., Rominger, A., Bartenstein, P., Schuff, N., ... Alzheimer's Disease Neuroimaging Initiative (ADNI). (2014). Reduced FDG-PET brain metabolism and executive function predict clinical progression in elderly healthy subjects. *NeuroImage Clinical*, 4, 45–52.
- Falahati, F., Ferreira, D., Soininen, H., Mecocci, P., Vellas, B., Tsolaki, M., ... AddNeuroMed consortium and the Alzheimer's Disease Neuroimaging Initiative. (2016). The effect of age correction on multivariate classification in Alzheimer's disease, with a focus on the characteristics of incorrectly and correctly classified subjects. *Brain Topography*, 29, 296–307.
- Fischl, B., Salat, D. H., Busa, E., Albert, M., Dieterich, M., Haselgrove, C., ... Dale, A. M. (2002). Whole brain segmentation: Automated labeling of neuroanatomical structures in the human brain. *Neuron*, 33, 341–355.
- Fischl, B., Sereno, M. I., & Dale, A. M. (1999). Cortical surface-based analysis. II: Inflation, flattening, and a surface-based coordinate system. *NeuroImage*, 9, 195–207.
- Gaser, C., Franke, K., Klöppel, S., Koutsouleris, N., Sauer, H., & Alzheimer's Disease Neuroimaging Initiative. (2013). BrainAGE in mild cognitive impaired patients: Predicting the conversion to Alzheimer's disease. *PLoS One*, 8, e67346.
- Hanseeuw, B. J., Betensky, R. A., Jacobs, H. I. L., Schultz, A. P., Sepulcre, J., Becker, J. A., ... Johnson, K. (2019). Association of amyloid and tau with cognition in preclinical Alzheimer disease: A longitudinal study. *JAMA Neurology*, 76(8), 915–924.
- Harms, M. P., Somerville, L. H., Ances, B. M., Andersson, J., Barch, D. M., Bastiani, M., ... Yacoub, E. (2018). Extending the human connectome project across ages: Imaging protocols for the lifespan development and aging projects. *NeuroImage*, 183, 972–984.
- Holland, D., Desikan, R. S., Dale, A. M., McEvoy, L. K., & for the Alzheimer's Disease Neuroimaging Initiative. (2012). Rates of decline in Alzheimer disease decrease with age. *PLoS One*, 7, e42325.
- Jack, C. R., Jr., Therneau, T. M., Weigand, S. D., Wiste, H. J., Knopman, D. S., Vemuri, P., ... Petersen, R. C. (2019). Prevalence of biologically vs clinically defined Alzheimer spectrum entities using the National Institute on Aging–Alzheimer's association research framework. *JAMA Neurology*, 76, 1174–1183.
- Jónsson, B. A., Björnsdóttir, G., Thorgeirsson, T. E., Ellingsen, L. M., Walters, G. B., Gudbjartsson, D. F., ... Ulfarsson, M. O. (2019). Brain age prediction using deep learning uncovers associated sequence variants. *Nature Communications*, 10, 1–10.
- Kaufmann, T., van der Meer, D., Doan, N. T., Schwarz, E., Lund, M. J., Agartz, I., ... Westlye, L. T. (2019). Common brain disorders are

- associated with heritable patterns of apparent aging of the brain. *Nature Neuroscience*, 22, 1617–1623.
- Knopman, D. S., Lundt, E. S., Therneau, T. M., Vemuri, P., Lowe, V. J., Kantarci, K., ... Jack, C. R., Jr. (2018). Joint associations of beta-amyloidosis and cortical thickness with cognition. *Neurobiology of Aging*, 65, 121–131.
- Koikkalainen, J., Pölönen, H., Mattila, J., van Gils, M., Soininen, H., Lötjönen, J., & for the Alzheimer's Disease Neuroimaging Initiative. (2012). Improved classification of Alzheimer's disease data via removal of nuisance variability. *PLoS One*, 7, e31112.
- Landau, S. M., Harvey, D., Madison, C. M., Koeppe, R. A., Reiman, E. M., Foster, N. L., ... Alzheimer's Disease Neuroimaging Initiative. (2011). Associations between cognitive, functional, and FDG-PET measures of decline in AD and MCI. *Neurobiology of Aging*, 32, 1207–1218.
- Landau, S. M., Mintun, M. A., Joshi, A. D., Koeppe, R. A., Petersen, R. C., Aisen, P. S., ... for the Alzheimer's Disease Neuroimaging Initiative. (2012). Amyloid deposition, hypometabolism, and longitudinal cognitive decline. *Annals of Neurology*, 72, 578–586.
- LaPoint, M. R., Chhatwal, J. P., Sepulcre, J., Johnson, K. A., Sperling, R. A., & Schultz, A. P. (2017). The association between tau PET and retrospective cortical thinning in clinically normal elderly. *NeuroImage*, 157, 612–622.
- Li, B., Zhang, M., Riphagen, J., Morrison Yochim, K., Li, B., Liu, J., ... Alzheimer's Disease Neuroimaging Initiative. (2020). Prediction of clinical and biomarker conformed Alzheimer's disease and mild cognitive impairment from multi-feature brain structural MRI using age-correction from a large independent lifespan sample. *NeuroImage Clinical*, 28, 102387.
- Liem, F., Varoquaux, G., Kynast, J., Beyer, F., Kharabian Masouleh, S., Huntenburg, J. M., ... Margulies, D. S. (2017). Predicting brain-age from multimodal imaging data captures cognitive impairment. *NeuroImage*, 148, 179–188.
- Lu, D., Popuri, K., Ding, G. W., Balachandar, R., Beg, M. F., & Alzheimer's Disease Neuroimaging Initiative. (2018). Multimodal and multiscale deep neural networks for the early diagnosis of Alzheimer's disease using structural MR and FDG-PET images. *Scientific Reports*, 8, 5697.
- Luo, N., Sui, J., Abrol, A., Lin, D., Chen, J., Vergara, V. M., ... Calhoun, V. D. (2020). Age-related structural and functional variations in 5,967 individuals across the adult lifespan. *Human Brain Mapping*, 41, 1725–1737.
- Morlini, I. (2006). On multicollinearity and concavity in some nonlinear multivariate models. *Statistical Methods and Applications*, 15, 3–26.
- Olsson, B., Lautner, R., Andreasson, U., Öhrfelt, A., Portelius, E., Bjerke, M., ... Zetterberg, H. (2016). CSF and blood biomarkers for the diagnosis of Alzheimer's disease: A systematic review and meta-analysis. *Lancet Neurology*, 15, 673–684.
- Pedregosa, F., Varoquaux, G., Gramfort, A., Michel, V., Thirion, B., Grisel, O., ... Duchesnay, É. (2011). Scikit-learn: Machine learning in python. *Journal of Machine Learning Research*, 12, 2825–2830.
- Pettigrew, C., Soldan, A., Zhu, Y., Wang, M. C., Brown, T., Miller, M., ... BIOCARD Research Team. (2017). Cognitive reserve and cortical thickness in preclinical Alzheimer's disease. *Brain Imaging and Behavior*, 11, 357–367.
- Qiu, S., Joshi, P. S., Miller, M. I., Xue, C., Zhou, X., Karjadi, C., ... Kolachalama, V. B. (2020). Development and validation of an interpretable deep learning framework for Alzheimer's disease classification. *Brain*, 143, 1920–1933.
- Salat, D. H., Buckner, R. L., Snyder, A. Z., Greve, D. N., Desikan, R. S., Busa, E., ... Fischl, B. (2004). Thinning of the cerebral cortex in aging. *Cerebral Cortex*, 14, 721–730.
- Salat, D. H., Lee, S. Y., van der Kouwe, A. J., Greve, D. N., Fischl, B., & Rosas, H. D. (2009). Age-associated alterations in cortical gray and white matter signal intensity and gray to white matter contrast. *NeuroImage*, 48, 21–28.
- Spasov, S., Passamonti, L., Duggento, A., Liò, P., Toschi, N., & Alzheimer's Disease Neuroimaging Initiative. (2019). A parameter-efficient deep learning approach to predict conversion from mild cognitive impairment to Alzheimer's disease. *NeuroImage*, 189, 276–287.
- Ten Kate, M., Barkhof, F., Visser, P. J., Teunissen, C. E., Scheltens, P., van der Flier, W. M., & Tijms, B. M. (2017). Amyloid-independent atrophy patterns predict time to progression to dementia in mild cognitive impairment. *Alzheimer's Research & Therapy*, 9, 73.
- Ten Kate, M., Redolfi, A., Peira, E., Bos, I., Vos, S. J., Vandenberghe, R., ... Barkhof, F. (2018). MRI predictors of amyloid pathology: Results from the EMIF-AD multimodal biomarker discovery study. *Alzheimer's Research & Therapy*, 10, 100.
- Voevodskaya, O., Pereira, J. B., Volpe, G., Lindberg, O., Stomrud, E., van Westen, D., ... Hansson, O. (2018). Altered structural network organization in cognitively normal individuals with amyloid pathology. *Neurobiology of Aging*, 64, 15–24.
- Wachinger, C., Salat, D. H., Weiner, M., Reuter, M., & for the Alzheimer's Disease Neuroimaging Initiative. (2016). Whole-brain analysis reveals increased neuroanatomical asymmetries in dementia for hippocampus and amygdala. *Brain*, 139, 3253–3266.
- Wirth, M., Oh, H., Mormino, E. C., Markley, C., Landau, S. M., & Jagust, W. J. (2013). The effect of amyloid β on cognitive decline is modulated by neural integrity in cognitively normal elderly. *Alzheimer's & Dementia*, 9, 687–698.e1.
- Yuan, Z., Pan, C., Xiao, T., Liu, M., Zhang, W., Jiao, B., ... Shen, L. (2019). Multiple visual rating scales based on structural MRI and a novel prediction model combining visual rating scales and age stratification in the diagnosis of Alzheimer's disease in the Chinese population. *Frontiers in Neurology*, 10, 93.

SUPPORTING INFORMATION

Additional supporting information may be found in the online version of the article at the publisher's website.

How to cite this article: Li, B., Jang, I., Riphagen, J., Almaktoom, R., Yochim, K. M., Ances, B. M., Bookheimer, S. Y., Salat, D. H., & For the Alzheimer's Disease Neuroimaging Initiative (2021). Identifying individuals with Alzheimer's disease-like brains based on structural imaging in the Human Connectome Project Aging cohort. *Human Brain Mapping*, 1–12. <https://doi.org/10.1002/hbm.25626>